JACS
JOURNAL OF THE AMERICAN CHEMICAL SOCIETY

Article

pubs.acs.org/JACS

An Adsorbate Discriminatory Gate Effect in a Flexible Porous Coordination Polymer for Selective Adsorption of CO_2 over C_2H_2

Maw Lin Foo,[†,+] Ryotaro Matsuda,[*,†,‡,§,∥] Yuh Hijikata,[⊥] Rajamani Krishna,[#] Hiroshi Sato,[†] Satoshi Horike,[▽] Akihiro Hori,[†,∥] Jingui Duan,[†] Yohei Sato,[∥,○] Yoshiki Kubota,[∥,○] Masaki Takata,[∥,¶] and Susumu Kitagawa[*,†,∥,▽]

[†]Institute for Integrated Cell-Material Sciences (WPI-iCeMS), Kyoto University, Yoshida, Sakyo-ku, Kyoto 606-8501, Japan

[‡]Department of Applied Chemistry, Graduate School of Engineering, Nagoya University, Chikusa-ku, Nagoya 464-8603, Japan

[§]Japan Science and Technology Agency (JST), PRESTO, 4-1-8 Honcho, Kawaguchi, Saitama 332-0012, Japan

[∥]RIKEN SPring-8 center, 1-1-1 Kouto, Sayo-cho, Sayo-gun, Hyogo 679-5148, Japan

[⊥]Institute of Transformative Bio-Molecules (WPI-ITbM), Nagoya University, Chikusa-ku, Nagoya 464-8602, Japan

[#]Van 't Hoff Institute for Molecular Sciences, University of Amsterdam, Science Park 904, 1098 XH Amsterdam, The Netherlands

[▽]Department of Synthetic Chemistry and Biological Chemistry, Graduate School of Engineering, Kyoto University, Katsura, Nishikyo-ku, Kyoto 615-8510, Japan

[○]Department of Physical Science, Graduate School of Science, Osaka Prefecture University, 1-1 Gakuen-cho, Naka-ku, Sakai, Osaka 599-8531, Japan

[¶]Institute of Multidisciplinary Research for Advanced Materials, Tohoku University, 2-1-1 Katahira, Aoba-ku, Sendai 980-8577, Japan

Supporting Information

ABSTRACT: The adsorptive separation of C_2H_2 and CO_2 via porous materials is nontrivial due to the close similarities of their boiling points and kinetic diameters. In this work, we describe a new flexible porous coordination polymer (PCP) [Mn(bdc)(dpe)] (H_2bdc = 1,4-benzenedicarboxylic acid, dpe = 1,2-di(4-pyridyl)ethylene) having zero-dimensional pores, which shows an adsorbate discriminatory gate effect. The compound shows gate opening type abrupt adsorption for C_2H_2 but not for CO_2, leading to an appreciable selective adsorption of CO_2 over C_2H_2 at near ambient temperature (273 K). The origin of this unique selectivity, as unveiled by in situ adsorption-X-ray diffraction experiments and density functional theory calculations, is due to vastly different orientations between the phenylene ring of bdc and each gas in the nanopores. The structural change by photochemical transformation of this PCP via [2 + 2] photodimerization leads to the removal of inverse CO_2/C_2H_2 selectivity, verifying the mechanism of the guest discriminatory gate effect.

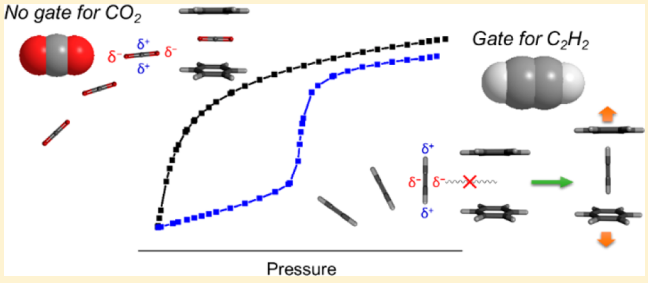

INTRODUCTION

There has been considerable interest in adsorptive separations involving separation of CO_2 from C_2H_2 due to its industrial relevance and scientific challenge. C_2H_2 is an industrial gas with applications such as oxyacetylene in welding/cutting and production of chemicals such as vinyl chloride, acrylic acid, and 1,4-butynediol.[1] In its manufacture via partial oxidation or hydrocarbon steam cracking of hydrocarbons, CO_2 is an important impurity. However, it is noted that the adsorptive separation of CO_2 (molecular size: 3.4 × 3.4 × 5.3 Å^3, bp 194.7 K) and C_2H_2 (molecular size: 3.4 × 3.4 × 5.5 Å^3, bp 189.3 K) is especially challenging due to their similarities in equilibrium sorption parameters, physicochemical properties, molecular size and shape (Table S1). In a few successful reports, porous materials were typically designed to preferentially adsorb C_2H_2 over CO_2 by utilizing adsorbent/adsorbate interactions via acid−base interaction at functional sites with highly polarizable π-electrons and acidic hydrogens on C_2H_2.[2] On the other hand, preferential adsorption of CO_2 over C_2H_2 (hereafter we call it "inverse selectivity")[3] is rarely observed above cryogenic temperatures, except recently in the case of a polyoxometallate hybrid ionic crystal.[4] However, the origins of the observed inverse selectivity were not well understood.

A unique characteristic of porous coordination polymers (PCPs) or metal−organic frameworks (MOFs)[5] from other conventional porous materials such as zeolites and porous carbons is structural flexibility[6] based on the concept of the soft

Received: October 7, 2015
Published: February 15, 2016

DOI: 10.1021/jacs.5b10491
J. Am. Chem. Soc. 2016, 138, 3022−3030

porosity,[7] providing unusual sorption behaviors. In particular, flexible PCPs in certain cases exhibit gated adsorption,[8] which is a unique phenomenon in which adsorption is negligible before a certain gate opening pressure (P_{go}), but at P_{go}, an abrupt increase in adsorption occurs due to a concomitant change in pore structure induced by structural distortion. Gated adsorption is one of the unique physical properties of PCPs with possible practical applications in selective adsorption[9] and sensing of gas molecules.[10] Although some recent studies have provided some guidelines in understanding and designing structural flexibility for controlling P_{go},[11] currently there is no clear strategy established for constructing a flexible PCP which shows gated adsorption for a specific guest molecule.

With this background, we target to construct a new PCP which shows gated adsorption for a specific guest molecule (acetylene) to achieve rational inverse selectivity. In our strategy, we utilize a PCP with small zero-dimensional (0-D) pores which will interact significantly differently with CO_2 and C_2H_2 due to the different signs of their quadrupole moments leading to different CH−π and π−π interactions.[12] Note that in larger pores, the same interactions might exist but will be markedly less in magnitude compared to isolated small 0-D pores.

Here, we show a design and synthesis of such a PCP as embodied by [Mn(bdc)(dpe)]⊃DMF (**1**⊃DMF) (where H_2bdc = 1,4-benzenedicarboxylic acid and dpe = 1,2-di(4-pyridyl)ethylene). **1′** (**1′** = desolvated **1**⊃DMF) shows gate opening type abrupt adsorption for C_2H_2 but not for CO_2 at low temperatures such as 195 K, leading to an appreciable selective adsorption of CO_2 over C_2H_2 at near ambient temperature (273 K). In addition, to verify the mechanism of selective gate opening behavior, [2 + 2] photodimerization on **1′** was employed for fine-tuning the spatial transformation of nanospace. Indeed, the photodimerized PCP [Mn_2(bdc)$_2$(*rctt*-tpcb)] (**2**) (where *rctt*-tpcb = *regio*−*cis*, *trans*, *trans*-tetrakis(4-pyridyl)cyclobutane) exhibits no selectivity because of the loss of efficient interaction between CO_2 and pore surface, verifying the mechanism of the guest discriminatory gate effect.

EXPERIMENTAL SECTION

All chemicals were used as received without any purification. Elemental analysis was obtained with a Flash EA 1112 elemental analyzer. ^{1}H NMR spectra were obtained with a 400 MHz Jeol ECA spectrometer. TGA data was collected with a ramp rate of 10 °C/min using a Rigaku TG8120 in flowing nitrogen. FT-IR spectra were collected using a Nicolet iD5 diamond ATR. Laboratory powder X-ray diffraction (PXRD) data were collected at ambient temperature on a Rigaku SmartLab X-ray diffractometer at 40 kV, 40 mA with Cu Kα radiation. Gas adsorption experiments were conducted between 77 K and ambient temperature using a Bel-max gas adsorption machine with adsorption temperatures maintained by a custom-made cryo apparatus from BEL, Inc. Samples of **1′** and **2** were activated at 120 °C overnight before gas adsorption measurements.

Powder Synthesis of 1⊃DMF. In an argon-filled MBraun glovebox, 37.5 mg of anhydrous $MnCl_2$ (Aldrich), 99.69 mg of H_2bdc (TCI), and 328 mg of dpe (Aldrich) were added to a 50 mL glass bottle. The bottle was then filled with 30 mL of anhydrous DMF/methanol (80/20 v/v) (Wako) and sealed with a Teflon lined cap. The bottle was then brought out of the glovebox and heated at 120 °C for 24 h. The bright yellow powder was then filtered in air and washed with DMF and dried under vacuum. Weight of product = 0.140 g, and yield is quantitative with respect to Mn. Elemental analysis calculated for $MnC_{23}H_{21}N_3O_5$: C, 58.23; H, 4.46; N, 8.86. Found: C, 57.55; H, 4.44; N, 8.59.

Powder Synthesis of 1′. **1**⊃DMF was heated at 180 °C for 5 h under dynamic vacuum to afford **1′**. It is stable and can be stored under ambient conditions. Elemental analysis calculated for $MnC_{20}H_{14}N_2O_4$: C, 59.86; H, 3.52; N, 6.98. Found: C, 60.61; H, 3.67; N, 7.04.

Single Crystals of 1⊃DMF. A volume of 0.5 mL of $MnClO_4$ solution in DMF (40 mM) was added to 0.5 mL of H_2bdc in DMF (40 mM) in a glass tube 0.3 cm in diameter. A buffer layer (0.5 mL) of DMF/MeOH (80/20 v/v) was then added carefully. Subsequently, 1 mL of dpe in MeOH (20 mM) was slowly added. The tube was then capped with a polypropylene cap and placed in an 80 °C oil-bath overnight. Yellow prism shaped crystals was observed and harvested by filtration and washing with DMF (see Table 1).

Table 1. Crystal Structure Data of 1⊃DMF and 1′

	1⊃DMF	1′
Empirical formula	$C_{43}H_{35}N_5O_9Mn_2$	$C_{20}H_{14}N_2O_4Mn$
Temperature (K)	223	223
Crystal system	Triclinic	Triclinic
Space group	$P\bar{1}$ (No. 2)	$P\bar{1}$ (No. 2)
a (Å)	10.0441(15)	9.2964(63)
b (Å)	10.5253(16)	10.1878(65)
c (Å)	11.3491(15)	12.0336(79)
V (Å^3)	1051.1(3)	993.3(11)
α (°)	78.453(8)	95.769(93)
β (°)	71.594(8)	99.637(32)
γ (°)	68.025(8)	115.6732(8)
Z	1	2
D_{cal} (g/cm^3)	1.383	1.342
μ (mm^{-1})	0.66	0.69
Total reflections corrected	5489	7475
Reflections unique	3504	3994
Restraints/parameters	0/344	0/244
GoF on F^2	1.256	1.225
R_1 indices [$I > 2\sigma(I)$]	0.1105	0.0581
R_1 indices (all data)	0.1126	0.0678
wR_2 (all data)	0.2503	0.1759

Photodimerization of 1′ Affording 2. Approximately 6 mg of **1′** in powder form was placed between two glass microscopic slides and these were taped shut. The slides were then placed in a Luz-Chem photoreactor with top and side lamps and irradiated with UV radiation (λ_{max} = 350 nm). After 24 h, the slides were flipped for irradiation of the opposite side. The slides were then untaped, and the powder was manually mixed with a spatula. Three such flipping and mixing cycles were performed to afford a yellowish-white powder **2**. Elemental analysis calculated for $MnC_{20}H_{16}N_2O_5$: C, 57.29; H, 3.85; N, 6.68. Found: C, 56.75; H, 3.87; N, 6.60.

Digestion of PCPs for Solution ^{1}H NMR. One milligram of **1**⊃DMF, **1′**, or **2** was dissolved in 2 mL of 10% aqueous Na_4EDTA (Aldrich) solution with the aid of sonication, followed by extraction (3 times) with 1 mL of CH_2Cl_2 (Wako) in a 5 mL glass vial. The combined CH_2Cl_2 extracts were evacuated, and the resulting white solid was dissolved in CD_2Cl_2.

Single Crystal X-ray Diffraction (XRD) Measurements. Measurements of **1**⊃DMF and **1′** were performed at 223 K with a Rigaku AFC10 diffractometer with Rigaku Saturn Kappa CCD system equipped with a MicroMax-007 HF/VariMax rotating-anode X-ray generator with confocal monochromated Mo Kα radiation. The crystal structure was solved by a direct method and refined by full matrix least-squares refinement using Superflip[13] for **1**⊃DMF and SHELXL-97[14] for **1′**. The hydrogen atoms were added via a riding model. For **1**⊃DMF, the crystal is a non-merohedral twin.

Synchrotron Powder XRD. Synchrotron powder XRD measurements were performed at SPring-8 (Hyogo, Japan) BL44B2 beamline with λ = 0.80046 Å. For in situ gas adsorption measurements, a sample

DOI: 10.1021/jacs.5b10491
J. Am. Chem. Soc. 2016, 138, 3022−3030

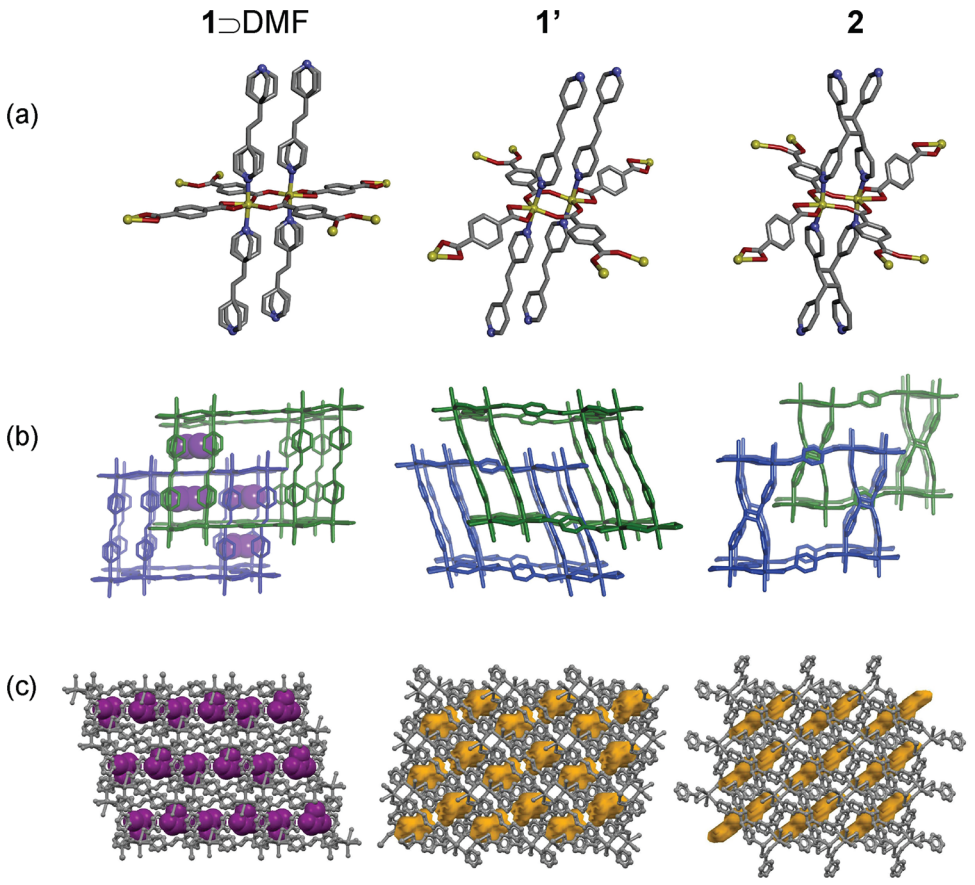

Figure 1. Crystal structures of **1**⊃DMF (left), **1**′ (center), **2** (right) with hydrogens omitted for clarity. (a) Coordination environment of Mn. For **1**⊃DMF, disordering in the pyridyl rings of dpe is present. Atoms are represented by colored spheres or sticks as Mn (yellow), O (red), N (blue), C (gray). (b) Box structural motif of **1**⊃DMF, **1**′, **2** with emphasis on the two-fold interpenetrated structure represented by blue and green. DMF molecules in **1**⊃DMF are represented by purple spheres. (c) The 3 × 3 × 3 unit cell emphasizing guest DMF molecules (purple spheres) for **1**⊃DMF and void volume (probe radius 1.2 Å) for **1**′ and **2**. Void space are visualized using Mercury CSD 2.0.[18]

of **1**′ was loaded into an open 0.4 mm glass capillary which was then connected to a custom-made gas-dosing apparatus (BEL Japan, Inc.). Synchrotron powder XRD of **1**′ and **2** at ambient was performed with a sealed 0.4 mm glass capillary.

In Situ Gas Adsorption−PXRD. In situ gas adsorption−PXRD measurements were carried out using a Rigaku SmartLab instrument with Cu Kα radiation connected to a BELSORP-18PLUS volumetric adsorption equipment (BEL Japan, Inc.). The apparatuses were automated and synchronized with each other, and each X-ray diffraction pattern was obtained at each equilibrium point in the adsorption isotherm.

Theoretical Calculations. To find the most favorable interactive site of CO_2 or C_2H_2 with the pore surface of **1**′, we evaluated the interaction energies between phenyl rings and CO_2 or C_2H_2 in various symmetrical configurations. The obtained energetically most favorable structures were employed as initial structures for optimization without symmetric restriction. All geometry optimizations were carried out using density functional theory (DFT) method with B3LYP functional[15] augmented with the Grimme's D_3 correction[16] for dispersion interaction. Basis set of cc-pVTZ was used for all atoms. Interaction energies were evaluated by MP2 and the same basis set with BSSE correction. All calculations were carried out with the Gaussian 09 program package.[17]

RESULTS AND DISCUSSION

The synthesis of microcrystalline powders of **1**⊃DMF was achieved via solvothermal synthesis. Single crystals were obtained by layering of DMF and methanol solutions with a mixed DMF/MeOH buffer layer in-between. From single crystal X-ray structural analysis, the asymmetric unit of **1**⊃DMF consists of one Mn^{2+} cation, one fully deprotonated bdc molecule, one disordered dpe molecule, and one DMF molecule. The formula of guest DMF was further verified by thermal gravimetric analysis (TGA), IR spectroscopy, and elemental analysis (Figures S1−S3). From TGA, **1**⊃DMF is thermally stable until 380 °C in flowing N_2. In the structure of **1**⊃DMF (Figure 1), Mn is located in a distorted octahedral environment, in the axial position; it is coordinated by two nitrogen atoms from dpe ligands, and in the equatorial position, it is coordinated by two oxygen atoms from one bdc in chelating mode and two other oxygen atoms from two different bdc in monodentate mode. The two bdc ligands link two Mn ions with μ-carboxylato fashion forming a Mn dimer cluster. The bond distances of the two crystallographically different Mn−N bonds are equivalent at 2.269 Å. The bond distances in Mn−O vary between 2.092 and 2.305 Å. The overall structure of **1**⊃DMF has a 2-fold interpenetrated box motif with α-Po topology. Each individual box motif consists of four Mn dimer clusters at each corner with Mn−Mn distances of 4.538 Å (Figure 1b). It is noted that the structure of **1**⊃DMF is similar to that of previously reported [Zn(bdc)(dpe)].[19] However, for this PCP, the binuclear Zn cluster is rotated by 90° at every other corner, whereas **1**⊃DMF has the same orientation throughout the crystal structure. **1**⊃DMF appears to have undulating 1-D channels along the [011] direction; however, the continuity of the 1-D channels is disrupted by the edges of

DOI: 10.1021/jacs.5b10491
J. Am. Chem. Soc. 2016, 138, 3022−3030

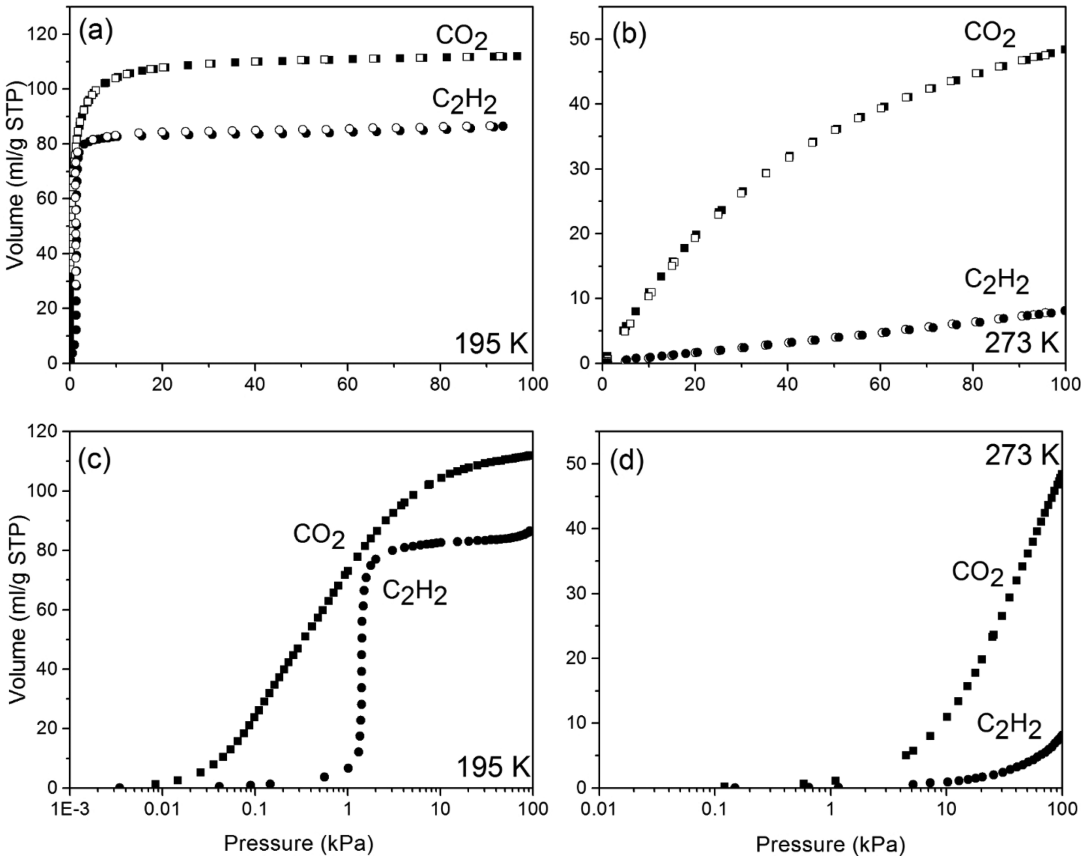

Figure 2. Sorption isotherms of **1**′ for CO_2 and C_2H_2. The isotherms are measured at (a and c) 195 and (b and d) 273 K; (a and b) presented with linear abscissae; (c and d) shown in logarithmic abscissae. Circles and squares represent C_2H_2 and CO_2, respectively. Close and open symbols represent adsorption and desorption, respectively.

the pyridyl rings from dpe resulting in the formation of isolated 0-D pores that are filled by one DMF molecule each (Figure 1c). It is noted that each DMF molecule is sandwiched between two phenylene rings from bdc with orthogonal orientation of the carboxylate group (Figure S4). The rings are almost eclipsed with distances from the centroid of each benzene ring to DMF ($N-C_{carbonyl}$) of 3.488 and 3.439 Å, respectively; this implies significant $\pi-\pi$ interactions between the two phenylene rings and DMF. After solvent removal with heating under vacuum to afford **1**′ (Figure 1), the structure undergoes distortion via shearing of the box structural motif with concurrent tilting of the dpe pillars (24°) and significant rotation of the phenylene ring of bdc with chelating mode (25° with respect to the mean plane defined by the four carboxylate oxygens). This rotation of the aromatic ring is the most important change because the tilted rings further reduced the volume of 0-D pore, resulting in the formation of dimers of kidney-shaped isolated porous structure (each with dimensions of approximately 3.3 × 3.5 × 5.6 $Å^3$) along the $[10\bar{1}]$ direction. Each 0-D pore is separated from each other due to the tilted rings from bdc and dpe. Thus, the pore system can be considered as undulating pseudo 1-D channels assembled by 0-D pores. The unit cell volume is reduced from the original as-synthesized 1051 to 993 $Å^3$. From Platon program, the void volume is calculated to be 17.4% (173 $Å^3$).

The gas adsorption properties of **1**′ were studied with respect to N_2 at 77 K, O_2, CO_2 and CH_4 at 195 K using a crystalline powder sample (Figure S5). For O_2, N_2, and CH_4, no appreciable adsorption could be observed due to the non-porosity of the pseudo-1-D channels for these gas molecules. However, **1**′ adsorbs 111 mL (STP)/g (1.97 mmol CO_2/mmol Mn or 21.6 wt %) of CO_2 at 195 K, which may be due to its smallest kinetic diameter (3.3 Å) enabling the access of CO_2 into the pseudo-1-D channels. It is noted that there are approximately 4 molecules of CO_2 per unit cell ($Z = 2$), in good agreement with the void volume of **1**. As **1**′ does not adsorb N_2 at 77 and 195 K (Figures S5 and S6), its surface area was calculated by CO_2 adsorption at 195 K using the Brunauer–Emmett–Teller (BET) model to afford a surface area of 535 m^2/g (Figure S7). The isosteric heat of adsorption, Q_{st} for CO_2 is calculated by the virial method to be 29–30 kJ/mol and does not change appreciably with loading (Figure S8), suggesting uniformity of binding sites. In addition, the Q_{st} for CO_2 of our compound is moderately high compared to MOFs with no open metal sites or polar functional groups such as MOF-508 $[Zn(bdc)(bpy)_{0.5}]$[20] (with Q_{st} of 16–20 kJ/mol).[21] From a practical standpoint, the constant and moderately high value of Q_{st} at different loadings renders **1**′ useful for the effective separations of CO_2 from other gases. The adsorption isotherm of C_2H_2 was obtained at 195 K (Figure 2a,c). Unlike the CO_2 case, a gated behavior (with P_{go} = 1.45 kPa) was clearly observed. Below the gate opening pressure, adsorption of C_2H_2 is negligible, but an abrupt increase is observed after P_{go} reaches 86.2 mL/g STP (1.55 mmol C_2H_2/mmol Mn). In sharp contrast, for CO_2 the gas uptake is increasing monotonically and no clear gate opening behavior was observed even at low pressure region. This behavior is markedly different from other 0-D frameworks such as

DOI: 10.1021/jacs.5b10491
J. Am. Chem. Soc. 2016, 138, 3022–3030

[Cu(etz)] (hetz = 3,5-diethyl-1,2,4-triazole) where gate opening pressures is observed for both CO_2 and C_2H_2.[22]

On increasing the adsorption temperature to 273 K (Figure 2b,d), for **1′**, P_{go} for C_2H_2 adsorption increases to greater than 1 atm; thus, adsorption (91 kPa, 7.3 mL/g STP) is negligible with linear adsorption profile, resulting in low heats of adsorption (Figure S9). In contrast, CO_2 is adsorbed smoothly even at 273 K (46.8 mL/g STP at 91 kPa) without gate opening behavior despite the considerably narrow paths in the pseudo-1-D channels.

The ratio of CO_2/C_2H_2 adsorbed at 90 kPa is 6.4, which suggests that **1′** is potentially useful for separating CO_2 from C_2H_2 with high selectivity at noncryogenic temperatures. It is noted that this ratio is the highest achieved until date for inverse selectivity of CO_2/C_2H_2 near room temperature (Table S2). To establish the feasibility of gas separations, the ideal adsorbed solution theory (IAST) calculations[23] were used to predict the separation of an equimolar amount of C_2H_2 and CO_2 from its pure isotherms at 273 K (Figure S10). The CO_2/C_2H_2 selectivity for an equimolar CO_2/C_2H_2 gas mixture varies from 8.8 to 13. The results from the IAST calculations indicate that **1′** may be suitable for practical use as a material for separating CO_2 from a CO_2/C_2H_2 mixture over a wide range of pressures at ambient temperature.

To evaluate the gas separation ability of adsorbents under kinetic gas conditions, breakthrough simulations were performed,[24] which are strongly pertinent to the pressure swing adsorption (PSA) process, an energetically efficient method for industrial scale separations. With the aid of transient breakthrough simulations, we aim to demonstrate that pure C_2H_2 can be produced during the adsorption phase in fixed-bed adsorbers. The performance of industrial fixed bed adsorbers is dictated by a combination of adsorption selectivity and working capacity. The breakthrough simulations were performed for a total gas pressure of 100 kPa, and constant temperature of 273 K. The transient breakthrough simulation results are presented in terms of a dimensionless time, τ, which is a metric determining the frequency of required regeneration and influencing the productivity of a PSA unit. Figure 3a presents the results for a 50/50 CO_2/C_2H_2 mixture. The *y*-axis in Figure 3a is the dimensionless concentration of each component normalized with respect to the concentration at the feed inlet concentration. We note that the separation is very sharp with the breakthrough curves for CO_2 and C_2H_2 showing near-vertical slopes. As C_2H_2 possesses low affinity to **1′**, it breaks through quickly and τ for CO_2 to break through is ~7−8 times longer. The ability of **1′** to selectively adsorb CO_2 is an important advantage of this flexible PCP/MOF as pure C_2H_2 can be produced during the "adsorption" phase of fixed-bed adsorption operations. Other PCPs/MOFs have been suggested in the literature as being suitable for separation of CO_2/C_2H_2 mixtures: (1) HOF-3 (a rod-packing 3D microporous hydrogen-bonded organic framework),[25] (2) HKUST-1 (= $Cu_3(BTC)_2$),[26] (3) ZJU-60a (= $Cu_2(MFDI)$),[27] (4) PCP-33,[28] and (5) MIL-100 (Fe).[29] All five of these PCPs/MOFs adsorb C_2H_2 selectively. As a consequence, pure C_2H_2 can only be produced in the "desorption" phase of fixed bed adsorber operations with these PCPs/MOFs. The attainment of high purity product in the desorption phase is considerably more difficult in fixed bed operations compared to obtaining the product via the adsorption phase.[30]

It is noted that for flexible PCPs/MOFs, despite some recent works,[31] there remains some controversy about their ability to separate mixtures since it can be reasoned that on adsorption of one component, the other component may be simultaneously adsorbed despite the appearance of their respective pure isotherms. To verify that **1′** can indeed separate C_2H_2 from a CO_2/C_2H_2 mixture, we have performed a trial gas separation experiment using a flowing 50/50 CO_2/C_2H_2 mixture at 100 kPa and 273 K. The results of the experiment (Figure 3b, Figure S11) show that CO_2 is selectively adsorbed from CO_2/C_2H_2 mixture as the gas composition of the adsorbed component is 85/15, whereas the flowing gas composition is 50/50. The partition coefficient is 5.7, which is greater than one, indicating that preferential adsorption of CO_2 does occur in the presence of C_2H_2.

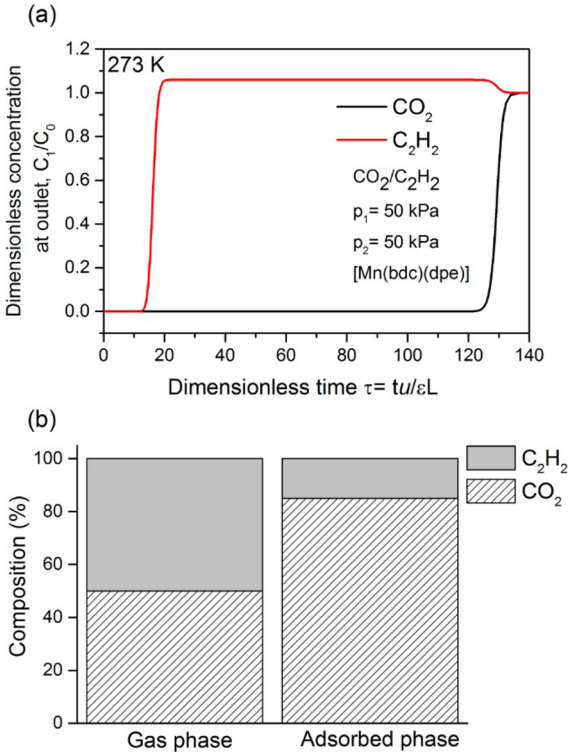

Figure 3. (a) Simulated breakthrough curve at 273 K for a 50/50 mixture of CO_2/C_2H_2 at 100 kPa. (b) Gas separation experiment results obtained by flowing 50/50 mixture of CO_2/C_2H_2 at 273 K, followed by ascertaining composition of adsorbed phase by gas chromatography.

To further understand temperature dependency of the adsorption behavior for CO_2 and C_2H_2, additional adsorption measurements were performed at different temperatures between 195 and 273 K. For C_2H_2, a steady increase in P_{go} with temperature is observed (Figure 4), consistent with previous observations in the literature.[32]

A linear plot is obtained by plotting the gate opening pressures vs inverse of temperature (Figure S12), similar to previous studies.[33] It is established that above 252 K, the gate opening pressure is larger than 100 kPa. For CO_2, no clear gate opening pressure is observed at any temperature, suggesting that adsorption of CO_2 is smooth with no difficulty in the diffusion of CO_2 molecules in pseudo-1-D channels.

To elucidate the reason for the presence of P_{go} for C_2H_2 but its absence in CO_2 adsorption, in situ adsorption coupled with X-ray diffraction experiments were performed (Figure 5).[34] Due to the triclinic symmetry and considerable overlap of peaks, complete indexing of the patterns could not be

DOI: 10.1021/jacs.5b10491
J. Am. Chem. Soc. 2016, 138, 3022−3030

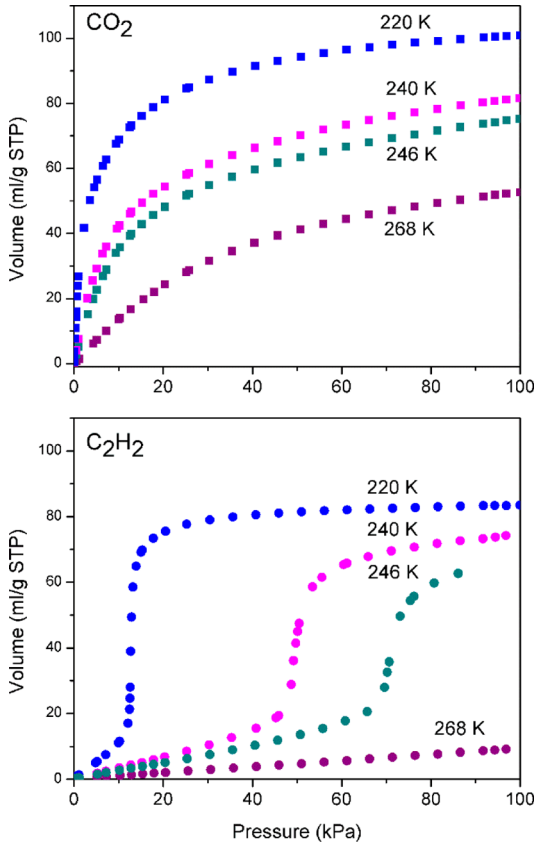

Figure 4. Adsorption isotherms of CO_2 (top) and C_2H_2 (bottom) for **1**′ at 220, 240, 246, and 268 K.

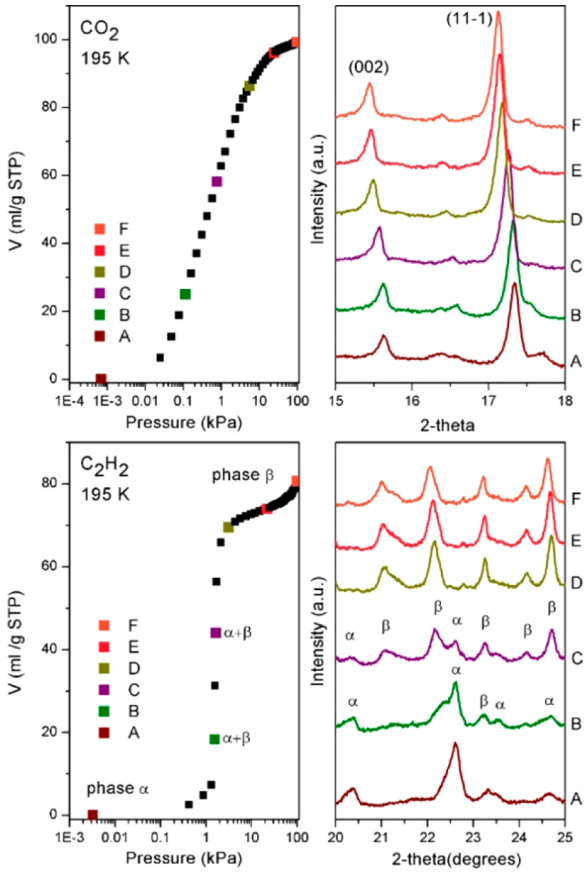

Figure 5. Adsorption isotherms and in situ adsorption-XRD of **1**′ for CO_2 at 195 K (top) and C_2H_2 at 195 K (bottom).

satisfactorily performed. However, significant difference in the X-ray diffraction patterns could be observed upon adsorption between CO_2 and C_2H_2. In the case of CO_2 adsorption, a continuous shift of peaks, especially for the two peaks indexed as (002) and $(11\bar{1})$ to lower angle region in the PXRD patterns, was seen, suggesting that the framework expands gradually in response to the increasing volume of CO_2 adsorbed. On the other hand, the in situ PXRD patterns for C_2H_2 show two main phases, α and β, which correspond to the closed phase before gate opening and the open form after gate opening, respectively. From Figure 5, it is evident that along the sharp vertical adsorption step (Figure 5, points B and C in the isotherm of C_2H_2), both α and β phases are present and their relative proportions (as elucidated by the intensity of the powder diffraction peaks) are in good agreement with the relative amount adsorbed.

In addition, attempts were made to obtain the lattice parameters of the gas-filled phases of **2** at 195 K via synchrotron radiation. For **1**⊃CO_2, a good Le Bail fit (Figure S13a) could be performed. The following lattice parameters were obtained: a = 9.6609(3) Å, b = 11.5232(4) Å, c = 10.5314(2) Å; α = 105.684(3)°, β = 114.898(2)°, γ = 81.211(2)°. The unit cell volume is 1023 Å^3, which is clearly larger than that of dried **1**′ (993 Å^3), consistent with occupation by gas molecules. However, for **1**⊃C_2H_2, the indexing was not very successful due to the complex PXRD pattern. Despite this limitation, the appearance of low angle peaks and the best indexing result (Figure S13b) suggests a much larger unit cell volume was obtained compared to **1**⊃CO_2, which implies a much larger structural change has occurred with approximately the same volume of gas adsorbed.

Once again, this unusual large difference in adsorption between CO_2 and C_2H_2 is unprecedented. As mentioned above, CO_2 and C_2H_2 have very similar size and physicochemical properties, but they possess opposite quadruple moment around rod shaped bodies. Therefore, to understand the large difference in gas adsorption for these two gases, we initially assumed that **1**′ should recognize the opposite quadruple moment of these two molecules. On the other hand, **1**′ has very small pores which can be classified as almost 0-D, as is described above. Both molecules cannot diffuse into the channels if we consider these gas molecules as rigid sphere model with kinetic diameters of 3.3 Å. However, they have rod-shaped anisotropic molecular dimensions. Hence, if the molecule thrusts into the pore in an end-on type fashion (principle axis along the channel direction), the minimum accessible size of pore should be much less than that of kinetic diameter, which may possibly allow CO_2 and C_2H_2 molecules to diffuse into such small pores. As the pores of **1**′ are quite small, its crystallographic structure suggests that the molecules cannot move around freely in the pore but are forced to keep its orientation during diffusion and adsorption unless a structural expansion occurs.

Consequently, our hypothesis of inverse adsorption selectivity is shown in Figure 6: the electrostatic potential formed in the small pore effectively interacts with the quadruple moment of CO_2 in an end-on orientation along the channel direction, resulting in the gradual and smooth adsorption (I, II) with a gradual change in cell parameters. On the other hand, the pore potential results in repulsive interaction with C_2H_2 in an end-on orientation because of the opposite quadruple

DOI: 10.1021/jacs.5b10491
J. Am. Chem. Soc. 2016, 138, 3022−3030

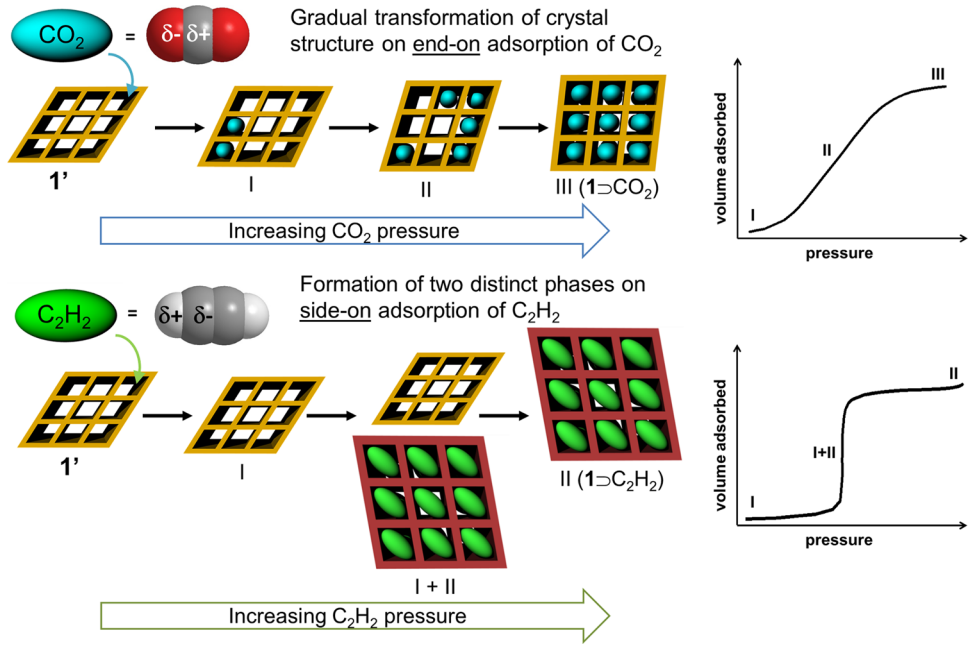

Figure 6. Possible adsorption mechanism of **1**′ for CO_2 (top, gradual transformation) and C_2H_2 (bottom, two-phase gated adsorption) at 195 K with corresponding adsorption isotherms. Note that the unit cell volume of **1**⊃C_2H_2 is much larger than that of **1**⊃CO_2 as revealed by in situ synchrotron X-ray diffraction.

moment, thus refusing access to C_2H_2 in the low pressure region (below P_{go} (I)) and requires large structural transformation to adsorb C_2H_2 with side-on orientation (principle axis perpendicular to the channel direction).

To prove our hypothesis, we first conducted DFT calculations whereupon a CO_2 or C_2H_2 molecule is inserted between two phenyl rings initially 6.924 Å apart, which is experimentally observed in **1**⊃DMF. The geometries are optimized by keeping the two phenyl rings in parallel. For CO_2, the distance shrinks to 6.575 Å with the most stable molecular configuration that CO_2 molecules are parallel to phenylene rings (i.e., keeping end-on access fashion). For C_2H_2, the most stable configuration is perpendicular to phenylene rings to maximize electrostatic interaction (CH−π interactions in this case), which requires pore expansion making the distance between phenylene rings 8.324 Å (Figure 7). This is consistent with our hypothesis that CO_2 tends to migrate into pores more smoothly, whereas C_2H_2 is refused without the occurrence of gate opening behavior.

Second, we obtained experimental evidence further supporting our proposed mechanism. As elucidated in the DFT calculation, the local flexibility of the phenylene rings plays an important role in the adsorption event. We expect that if we could induce changes in the orientation of the phenyl rings in **1**′, such as tilting against channel direction, effective interaction between the phenylene plane and guest molecules is rendered highly impossible, which could result in destroying the adsorption selectivity.

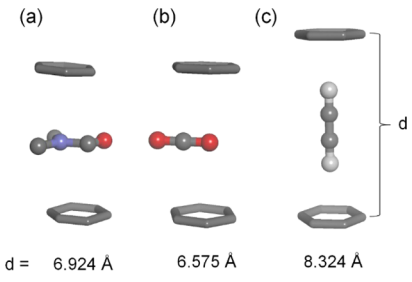

Figure 7. Distance between the centroids of two stacked benzene rings (a) as experimentally observed in **1**⊃DMF. As optimized by DFT calculations for (b) CO_2 and (c) C_2H_2.

To realize such structural change, we attempted [2 + 2] photodimerization of the dpe ligands to ascertain its effect on the conformation of phenyl rings. This is due to two reasons: First, the dpe pillars seem to be key for structural flexibility due to differences of the tilt angle in **1** and **1**′. Second, [2 + 2] photodimerization is highly feasible because the ethylenic carbons in **1**′ at each corner of the box motif are eclipsed at a distance of 4.024 Å apart, which fulfills Schimdt's criterion[35] (<4.2 Å).

After exposing **1**′ to UV (λ_{max} = 350 nm) irradiation for 1 week, powders of **1**′ changed significantly from bright yellow to whitish-yellow (Figure S14). In comparison to Zn coordination polymers, [2 + 2] photodimerization of Mn coordination polymers is relatively rare.[36] The color change strongly suggests that the conjugation of Mn−dpe−Mn system has been lost via photodimerization. Digestion of the photoirradiated product followed by ^{1}H NMR and mass spectrometry (Figures S15 and S16) verified the quantitative dimerization to tetrakis(4-pyridyl)cyclobutane (tpcb) by the complete disappearance of the olefin protons at δ = 7.25 ppm and shifting of the two pyridyl protons with peaks centered at δ = 7.43, 8.60 ppm. It is noted that only one set of cyclobutane protons is observed at δ = 4.48 ppm. Thus, the [2 + 2] photodimerization is completely regioselective as only the *rctt* isomer is present.[37] Hence, **1**′ has undergone [2 + 2] photodimerization to form **2** (Figure 8). From TGA (Figure S17), the thermal stability of **2** did not differ appreciably from that of **1**′.

Because of severe deterioration of single crystallinity upon the photodimerization from **1**′ to **2**, structural determination of the photodimerized compound **2** was unsuccessful. However,

DOI: 10.1021/jacs.5b10491
J. Am. Chem. Soc. 2016, 138, 3022−3030

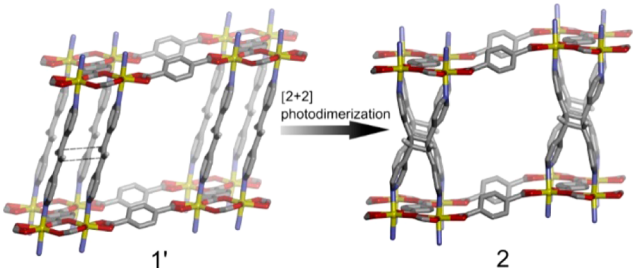

Figure 8. Transformation of **1′** into **2** via [2 + 2] photodimerization of the coordinated dpe ligands. For simplicity, the two-fold interpenetration in the both structures is neglected and only a single box motif is considered. Aromatic protons are excluded for clarity. The dotted lines in **1′** indicate the eclipsed C═C bonds with distances of 4.024 Å.

we could successfully obtain the crystal structure of **2** from performing a Rietveld analysis with high reliability (R_{wp} of 3.64%) on a high quality synchrotron XRD pattern (Figures S18 and S19) using a preliminary dimerized structure optimized with molecular mechanics[38] from the structure of **2** (Figure 1); it is observed that the unit cell volume of **2** is slightly reduced from 993 to 981 Å^3. Due to the pyridyl rings displacing closer to each other for the dimerization to occur, the nearly linear Mn−N−Mn bond angle is distorted from 177° in **1′** to 164° in **2**. In addition, the Mn−Mn distance is now lengthened to 4.287 Å. Interestingly, the tilt of the bdc phenyl rings in the chelating mode is also significantly increased from the original 25 to 45°.

Although the porosity of **2** is almost similar to that of **1′** (17.5%, 172 Å^3), which was also confirmed by a Type I isotherm of O_2 at 90 K (Figure S20), now all adjacent 0-D kidney-shaped pores are merged and flattened to afford a single cigar-shaped pore of 2.7 × 3.4 × 13.5 Å^3. Interestingly, in the CO_2 gas adsorption isotherm at 273 K for **2** (Figure 9), it is

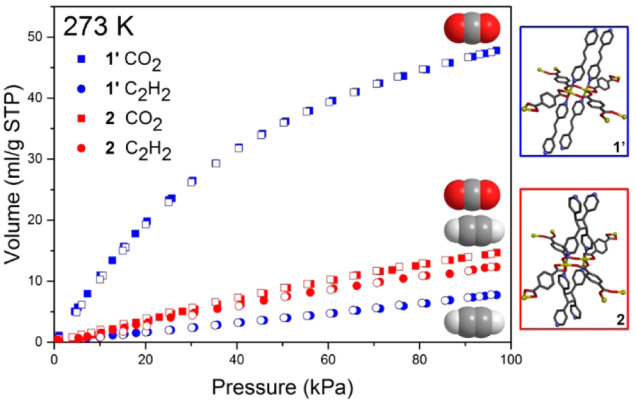

Figure 9. Gas sorption isotherms for CO_2 and C_2H_2 for **1′** (blue) and **2** (red) at 273 K. Squares represent CO_2 and circles C_2H_2. Open symbols represent adsorption and closed symbols desorption.

observed that its profile is linear with a significant decrease in uptake compared to the case for **1′**. In addition, the uptake of CO_2 (14.1 mL/g STP) and C_2H_2 (11.8 mL/g STP) at 91 kPa for **2** is now almost identical. This indicates that after photodimerization, in the pores of the resultant PCP, CO_2 molecules cannot interact with phenylene rings efficiently because of the significant tilting of phenylene rings upon photodimerization, resulting in the loss of its inverse selectivity for CO_2/C_2H_2 and its sorption behavior. It is noted that the ethylenic double bonds in **1′** are not lining the pore surface; thus, they are not contributing to adsorption selectivity. This result strongly supports the proposed mechanism of the inversed selectivity in **1′** based on the guest discriminatory gated effect.

CONCLUSIONS

In conclusion, we have demonstrated an alternative concept for separating gases with similar size and physical properties. In contrast to conventional approaches such as strong chemical interactions and/or molecular sieving, our approach entails selecting a soft framework with narrow 0-D pores, which will selectively exhibit gate opening behavior for one of the components due to differences in electronic properties. For such an approach to work, the pores must be narrow leading to the gas molecules possessing intimate contact with the pore environment. In addition, the gas molecules should possess distinctly different electronic properties, i.e., CO_2 and C_2H_2 have quadrupole moment of different signs resulting in (thus requiring) different distortions of the pore environment. It is noted that in this instance, both global (change in crystal structure) and local (tilt in phenylene ring of bdc) flexibility are important for showing the selective gate opening behavior for C_2H_2.

As the gate opening pressure increases with temperature, the selectivity of separation will increase with increasing temperature. This is seen in the sorption behavior of **1′** and leads to the clear manifestation of inverse selectivity—the preferential adsorption of CO_2 over C_2H_2 at 273 K. As refrigeration is both expensive and energy intensive, separations close to ambient temperatures will be increasingly important for industrial applications. We have demonstrated the feasibility of this with a preliminary gas separation experiment under flowing conditions using a 50/50 CO_2/C_2H_2 gas mixture.

ASSOCIATED CONTENT

Supporting Information

The Supporting Information is available free of charge on the ACS Publications website at DOI: 10.1021/jacs.5b10491.

^{1}H NMR, XRD, TGA, IR of **1**, **1′** and **2** (PDF)

X-ray crystallographic file of **1** (CCDC 1008212), **1′** (CCDC 1008213), and **2** (CCDC 1048123) (CIF)

Movie with further information on the breakthrough simulation for 50/50 CO_2/C_2H_2 gas mixture at 100 kPa (MPG)

AUTHOR INFORMATION

Corresponding Authors

*ryotaro.matsuda@apchem.nagoya-u.ac.jp

*kitagawa@icems.kyoto-u.ac.jp

Present Address

[+]National University of Singapore, Department of Chemistry, 3 Science Drive 3, Singapore 117543.

Notes

The authors declare no competing financial interest.

ACKNOWLEDGMENTS

We thank Dr. Hiroyasu Sato from Rigaku Corporation, Japan for his assistance in solving the crystal structure of **1**. T. Nishijima and T. Fuke provided expert technical support. This

DOI: 10.1021/jacs.5b10491
J. Am. Chem. Soc. 2016, 138, 3022−3030

work is supported by the PRESTO and ACCEL project of the Japan Science and Technology Agency (JST), and JSPS KAKENHI Grant-in-Aid for Young Scientists (B) (Grant No. 25870360), for Challenging Exploratory Research (Grant No. 25620187) and for Specially Promoted Research (Grant No. 25000007). This work was also supported in part by the New Energy and Industrial Technology Development Organization (NEDO). iCeMS and ITbM is supported by the World Premier International Research Initiative (WPI) of the Ministry of Education, Culture, Sports, Science and Technology, Japan (MEXT).

REFERENCES

(1) (a) Pässler, P.; Hefner, W.; Buckl, K.; Meinass, H.; Meiswinkel, A.; Wernicke, H.-J.; Ebersberg, G.; Müller, R.; Bässler, J.; Behringer, H.; Mayer, D. *Ullmann's Encyclopedia of Industrial Chemistry*; Wiley-VCH Verlag GmbH & Co. KGaA, 2000. (b) Gannon, R. E. *Kirk-Othmer Encyclopedia of Chemical Technology*; John Wiley & Sons, Inc., 2000.

(2) Matsuda, R.; Kitaura, R.; Kitagawa, S.; Kubota, Y.; Belosludov, R. V.; Kobayashi, T. C.; Sakamoto, H.; Chiba, T.; Takata, M.; Kawazoe, Y.; Mita, Y. *Nature* **2005**, *436*, 238.

(3) Yang, W.; Davies, A. J.; Lin, X.; Suyetin, M.; Matsuda, R.; Blake, A. J.; Wilson, C.; Lewis, W.; Parker, J. E.; Tang, C. C.; George, M. W.; Hubberstey, P.; Kitagawa, S.; Sakamoto, H.; Bichoutskaia, E.; Champness, N. R.; Yang, S.; Schroder, M. *Chem. Sci.* **2012**, *3*, 2993.

(4) Eguchi, R.; Uchida, S.; Mizuno, N. *Angew. Chem., Int. Ed.* **2012**, *51*, 1635.

(5) (a) Kitagawa, S.; Kitaura, R.; Noro, S.-i. *Angew. Chem., Int. Ed.* **2004**, *43*, 2334. (b) Janiak, C.; Vieth, J. K. *New J. Chem.* **2010**, *34*, 2366. (c) Furukawa, H.; Cordova, K. E.; O'Keeffe, M.; Yaghi, O. M. *Science* **2013**, *341*, 1230444. (d) Rowsell, J. L. C.; Yaghi, O. M. *Microporous Mesoporous Mater.* **2004**, *73*, 3. (e) Li, J.-R.; Sculley, J.; Zhou, H.-C. *Chem. Rev.* **2012**, *112*, 869.

(6) (a) Uemura, K.; Matsuda, R.; Kitagawa, S. *J. Solid State Chem.* **2005**, *178*, 2420. (b) Ferey, G.; Serre, C. *Chem. Soc. Rev.* **2009**, *38*, 1380. (c) Schneemann, A.; Bon, V.; Schwedler, I.; Senkovska, I.; Kaskel, S.; Fischer, R. A. *Chem. Soc. Rev.* **2014**, *43*, 6062.

(7) Horike, S.; Shimomura, S.; Kitagawa, S. *Nat. Chem.* **2009**, *1*, 695.

(8) Kitaura, R.; Seki, K.; Akiyama, G.; Kitagawa, S. *Angew. Chem., Int. Ed.* **2003**, *42*, 428. (b) Li, D.; Kaneko, K. *Chem. Phys. Lett.* **2001**, *335*, 50.

(9) (a) Xiao, B.; Byrne, P. J.; Wheatley, P. S.; Wragg, D. S.; Zhao, X. B.; Fletcher, A. J.; Thomas, K. M.; Peters, L.; Evans, J. S. O.; Warren, J. E.; Zhou, W. Z.; Morris, R. E. *Nat. Chem.* **2009**, *1*, 289. (b) Henke, S.; Schneemann, A.; Wütscher, A.; Fischer, R. A. *J. Am. Chem. Soc.* **2012**, *134*, 9464.

(10) Yanai, N.; Kitayama, K.; Hijikata, Y.; Sato, H.; Matsuda, R.; Kubota, Y.; Takata, M.; Mizuno, M.; Uemura, T.; Kitagawa, S. *Nat. Mater.* **2011**, *10*, 787.

(11) (a) Ma, S.; Sun, D.; Wang, X.-S.; Zhou, H.-C. *Angew. Chem., Int. Ed.* **2007**, *46*, 2458. (b) Nijem, N.; Wu, H.; Canepa, P.; Marti, A.; Balkus, K. J.; Thonhauser, T.; Li, J.; Chabal, Y. J. *J. Am. Chem. Soc.* **2012**, *134*, 15201.

(12) (a) Witte, J.; Neaton, J. B.; Head-Gordon, M. *J. Chem. Phys.* **2014**, *140*, 104707. (b) Majumder, M.; Mishra, B. K.; Sathyamurthy, N. *Chem. Phys. Lett.* **2013**, *557*, 59.

(13) Oszlanyi, G.; Suto, A. *Acta Crystallogr., Sect. A: Found. Crystallogr.* **2005**, *61*, 147.

(14) Sheldrick, G. *Acta Crystallogr., Sect. A: Found. Crystallogr.* **2008**, *64*, 112.

(15) (a) Becke, A. D. *J. Chem. Phys.* **1993**, *98*, 5648. (b) Lee, C.; Yang, W.; Parr, R. G. *Phys. Rev. B: Condens. Matter Mater. Phys.* **1988**, *37*, 785.

(16) Grimme, S.; Antony, J.; Ehrlich, S.; Krieg, H. *J. Chem. Phys.* **2010**, *132*, 154104.

(17) Frisch, M. J.; Trucks, G. W.; Schlegel, H. B.; Scuseria, G. E.; Robb, M. A.; Cheeseman, J. R.; Scalmani, G.; Barone, V.; Mennucci, B.; Petersson, G. A.; Nakatsuji, H.; Caricato, M.; Li, X.; Hratchian, H. P.; Izmaylov, A. F.; Bloino, J.; Zheng, G.; Sonnenberg, J. L.; Hada, M.; Ehara, M.; Toyota, K.; Fukuda, R.; Hasegawa, J.; Ishida, M.; Nakajima, T.; Honda, Y.; Kitao, O.; Nakai, H.; Vreven, T.; Montgomery Jr., J. A.; Peralta, J. E.; Ogliaro, F.; Bearpark, M. J.; Heyd, J.; Brothers, E. N.; Kudin, K. N.; Staroverov, V. N.; Kobayashi, R.; Normand, J.; Raghavachari, K.; Rendell, A. P.; Burant, J. C.; Iyengar, S. S.; Tomasi, J.; Cossi, M.; Rega, N.; Millam, N. J.; Klene, M.; Knox, J. E.; Cross, J. B.; Bakken, V.; Adamo, C.; Jaramillo, J.; Gomperts, R.; Stratmann, R. E.; Yazyev, O.; Austin, A. J.; Cammi, R.; Pomelli, C.; Ochterski, J. W.; Martin, R. L.; Morokuma, K.; Zakrzewski, V. G.; Voth, G. A.; Salvador, P.; Dannenberg, J. J.; Dapprich, S.; Daniels, A. D.; Farkas, Ö.; Foresman, J. B.; Ortiz, J. V.; Cioslowski, J.; Fox, D. J. *Gaussian 09*; Gaussian, Inc.: Wallingford, CT, 2009.

(18) Macrae, C. F.; Bruno, I. J.; Chisholm, J. A.; Edgington, P. R.; McCabe, P.; Pidcock, E.; Rodriguez-Monge, L.; Taylor, R.; van de Streek, J.; Wood, P. A. *J. Appl. Crystallogr.* **2008**, *41*, 466.

(19) Mir, M. H.; Koh, L. L.; Tan, G. K.; Vittal, J. J. *Angew. Chem., Int. Ed.* **2010**, *49*, 390.

(20) Chen, B.; Liang, C.; Yang, J.; Contreras, D. S.; Clancy, Y. L.; Lobkovsky, E. B.; Yaghi, O. M.; Dai, S. *Angew. Chem., Int. Ed.* **2006**, *45*, 1390.

(21) Bastin, L.; Bárcia, P. S.; Hurtado, E. J.; Silva, J. A. C.; Rodrigues, A. E.; Chen, B. *J. Phys. Chem. C* **2008**, *112*, 1575.

(22) Zhang, J.-P.; Chen, X.-M. *J. Am. Chem. Soc.* **2009**, *131*, 5516.

(23) (a) Myers, A. L.; Prausnitz, J. M. *AIChE J.* **1965**, *11*, 121. (b) Babarao, R.; Hu, Z.; Jiang, J.; Chempath, S.; Sandler, S. I. *Langmuir* **2007**, *23*, 659.

(24) (a) Krishna, R. *Microporous Mesoporous Mater.* **2014**, *185*, 30. (b) Krishna, R. *RSC Adv.* **2015**, *5*, 52269.

(25) Li, P.; He, Y.; Zhao, Y.; Weng, L.; Wang, H.; Krishna, R.; Wu, H.; Zhou, W.; O'Keeffe, M.; Han, Y.; Chen, B. *Angew. Chem., Int. Ed.* **2015**, *54*, 574.

(26) Xiang, S.; Zhou, W.; Gallegos, J. M.; Liu, Y.; Chen, B. *J. Am. Chem. Soc.* **2009**, *131*, 12415.

(27) Duan, X.; Zhang, Q.; Cai, J.; Yang, Y.; Cui, Y.; He, Y.; Wu, C.; Krishna, R.; Chen, B.; Qian, G. *J. Mater. Chem. A* **2014**, *2*, 2628.

(28) Duan, J.; Jin, W.; Krishna, R. *Inorg. Chem.* **2015**, *54*, 4279.

(29) Yoon, J. W.; Lee, J. S.; Lee, S.; Cho, K. H.; Hwang, Y. K.; Daturi, M.; Jun, C.-H.; Krishna, R.; Chang, J.-S. *Chem. - Eur. J.* **2015**, *21*, 18431.

(30) (a) Krishna, R. *RSC Adv.* **2015**, *5*, 52269. Da Silva, F. A.; Rodrigues, A. E. *AIChE J.* **2001**, *47*, 341. (b) Grande, C. A.; Poplow, F.; Rodrigues, A. E. *Sep. Sci. Technol.* **2010**, *45*, 1252.

(31) (a) Li, L.; Krishna, R.; Wang, Y.; Yang, J.; Wang, X.; Li, J. *J. Mater. Chem. A* **2016**, *4*, 751. (b) Li, L.; Wang, Y.; Yang, J.; Wang, X.; Li, J. *J. Mater. Chem. A* **2015**, *3*, 22574. (c) Sato, H.; Kosaka, W.; Matsuda, R.; Hori, A.; Hijikata, Y.; Belosludov, R. V.; Sakaki, S.; Takata, M.; Kitagawa, S. *Science* **2014**, *343*, 167.

(32) (a) Kanoh, H.; Kondo, A.; Noguchi, H.; Kajiro, H.; Tohdoh, A.; Hattori, Y.; Xu, W.-C.; Moue, M.; Sugiura, T.; Morita, K.; Tanaka, H.; Ohba, T.; Kaneko, K. *J. Colloid Interface Sci.* **2009**, *334*, 1. (b) Aguado, S.; Bergeret, G.; Titus, M. P.; Moizan, V.; Nieto-Draghi, C.; Bats, N.; Farrusseng, D. *New J. Chem.* **2011**, *35*, 546.

(33) Yamazaki, T.; Takahashi, Y.; Yoshida, D. *J. Colloid Interface Sci.* **2011**, *362*, 463.

(34) Bureekaew, S.; Sato, H.; Matsuda, R.; Kubota, Y.; Hirose, R.; Kim, J.; Kato, K.; Takata, M.; Kitagawa, S. *Angew. Chem., Int. Ed.* **2010**, *49*, 7660.

(35) Cohen, M. D.; Schmidt, G. M. J.; Sonntag, F. I. *J. Chem. Soc.* **1964**, 2000.

(36) Yang, S.-Y.; Deng, X.-L.; Jin, R.-F.; Naumov, P.; Panda, M. K.; Huang, R.-B.; Zheng, L.-S.; Teo, B. K. *J. Am. Chem. Soc.* **2014**, *136*, 558.

(37) Vansant, J.; Toppet, S.; Smets, G.; Declercq, J. P.; Germain, G.; Van Meerssche, M. *J. Org. Chem.* **1980**, *45*, 1565.

(38) *Materials Studio Modeling Environment*, v6.0.0; Accelrys Software Inc., S. D., 2011.

DOI: 10.1021/jacs.5b10491
J. Am. Chem. Soc. 2016, 138, 3022−3030